Signatures of nonlinear dynamics

in an idealized atmospheric model

Dmitri Kondrashov *

Department of Atmospheric and Oceanic Sciences and Institute of Geophysics and Planetary Physics

University of California, Los Angeles, U.S.A.

Sergey Kravtsov

Department of Mathematical Sciences, Atmospheric Sciences Group, University of Wisconsin-Milwaukee, U.S.A.

Michael Ghil

Department of Atmospheric and Oceanic Sciences and Institute of Geophysics and Planetary Physics

University of California, Los Angeles, U.S.A.

Geosciences Department and Laboratoire de Météorologie Dynamique (CNRS and IPSL),

Ecole Normale Supérieure, F-75231 Paris Cedex 05, FRANCE

* *Corresponding author address: Department of Atmospheric and Oceanic Sciences, 405 Hilgard Ave, Box 951565, 7127 Math Sciences Bldg. UCLA Los Angeles, CA, 90095-1565, U.S.A.*

E-mail: dkondras@atmos.ucla.edu

ABSTRACT

Signatures of nonlinear dynamics are analyzed by studying the phase-space tendencies of a global baroclinic, quasi-geostrophic, three-level (QG3) model with topography. Nonlinear, stochastic, low-order prototypes of the full QG3 model are constructed in the phase space of this model's empirical orthogonal functions using the empirical model reduction (EMR) approach. The phase-space tendencies of the EMR models closely match the full QG3 model's tendencies. The component of these tendencies that is not linearly parameterizable is shown to be dominated by the interactions between "resolved" modes, rather than by multiplicative "noise" associated with unresolved modes. The way of defining the leading, resolved modes and the interactions between them plays a key role in understanding the nature of the QG3 model's dynamics, whether linear or nonlinear, deterministic or stochastic.

1. Introduction and motivation

We are interested here in the nonlinear dynamics of planetary waves in fairly realistic, high-dimensional atmospheric models. A promising way of better understanding this dynamics is to investigate the properties of state-averaged trajectories in a low-dimensional subspace of the full model's phase space. The mean, that is state-averaged, phase-space tendencies describe long-term preferred motion in the observed or simulated atmosphere and can possibly be related to transitions between distinct weather regimes (Selten and Branstator 2004). These tendencies depend on the climate state; they can be used to identify signatures of linear and nonlinear dynamics in intermediate models (Selten and Branstator 2004; Franzke et al. 2007), as well as in more highly resolved atmospheric general circulation models (AGCMs; Branstator and Berner 2005).

Branstator and Berner (2005) studied mean phase-space tendencies in version 0 of the Community Climate Model (CCM0). They projected the results of 280 integrations of CCM0, each of which was 50–100 simulated days long, onto a basis of empirical orthogonal functions (EOFs) and considered the dynamics in the six planes, each spanned by two of the four leading EOFs. These authors found that linear inverse models (LIMs; Penland, 1996) can describe relatively well the mean tendencies in some of these planes. For other planes, though, there were strong departures from linearity, such as a distinctive signature of "double swirls" in the diagnosed, two-dimensional (2-D) tendencies, and LIMs were clearly not adequate.

Franzke et al. (2007) analyzed the mean phase-space tendencies of Marshall and Molteni's (1993) global baroclinic, quasi-geostrophic, three-level (QG3) model with topography. They

projected the model equations onto a finite vector space spanned by the energy-norm EOFs, and defined the "resolved" modes as the EOF pair spanning any 2-D plane under consideration, while the rest of the EOFs were designated as the "unresolved" modes.

By using time series from a long integration of the full QG3 model, Franzke et al. (2007) decomposed the phase-space tendencies into several components; they did so by computing state averages of the instantaneous tendencies due to linear and nonlinear terms in the full QG3 model's equations. The nonlinear tendencies were further divided into those contributed either by the "bare-truncation," i.e. resolved modes, or by the unresolved modes; the latter contributions were interpreted as being due to additive or multiplicative noise, along the lines of the Majda–Timofeyev–Vanden-Eijnden (MTV) classification (Majda et al. 2003). Franzke et al. (2007) concluded that the contributions of the unresolved modes are crucial in forming the double-swirl patterns of mean tendencies in the QG3 model.

In this study, we aim to revisit the significance of various contributions — from resolved and unresolved modes — that lead to signatures of nonlinear dynamics by using an alternative, empirical way of defining the nonlinear interactions between the resolved and unresolved modes. Our approach differs in both its spirit and its methodology from state averaging the full QG3 model's instantaneous tendencies, as in Franzke et al. (2007). We will also quantify the sensitivity of the mean phase-space tendency attribution to the number of "resolved" modes considered.

Our procedure involves as its first, preliminary step the construction of a low-order model in the phase space of the full QG3 model's EOFs by using the empirical model reduction (EMR) methodology of Kravtsov et al. (2005, 2009) and Kondrashov et al. (2005, 2006). The EMR methodology models statistically the daily increments — called, hereafter, daily

tendencies — of the reduced state vector as a quadratic function of the state vector itself; it includes stochastic forcing to parameterize the effect of the modes not explicitly present in the deterministic EMR operator.

We will show first that long EMR simulation produces an excellent match to the QG3 model's mean daily tendencies; see also Kondrashov et al. (2006). We are thus in a position to explicitly identify the terms in the EMR model's dynamical operator that dominate contributions to nonlinear, double-swirl patterns in the QG3 model's mean tendencies. In particular, we will investigate various ways to define the resolved modes among the QG3 model's leading EOFs. Subsequently, we will give a dynamic interpretation of the mean phase-space tendencies of the EMR model, as resulting from interactions between either the resolved modes or between them and the unresolved ones. The analysis of state-averaged, EMR-parameterized daily tendencies will lead to very different conclusions than those obtained from Franzke et al. (2007). state-averaging of the QG3 model's instantaneous tendencies.

In Section 2, we briefly review the EMR formulation. In Section 3, we present the detailed budget analysis of the estimated tendencies. The results are summarized in Section 4.

2. Empirical model reduction (EMR)

EMR models formally belong to a class of multivariate, parametric stochastic models. They extend LIMs by including quadratic — and higher-order polynomial, if necessary — combinations of predicted variables in the empirical dynamical operator, and by adopting a multi-level approach in modeling the noise; the latter approach allows us to deal efficiently with correlated residual noise (Kravtsov et al. 2005, 2009).

We consider N regularly sampled observations of the state vector $\mathbf{x}(t) = \{x_i(t) : i = 1, ..., M;\ t = 1, ..., N$

$\mathbf{x}(t)$ is represented in this study by M leading principal components of the QG3 model's streamfunction. The main level of the EMR equations for modeling the increments Δx_i is:

$$\Delta x_i = (N_{ijk} x_j x_k + L^{(0)}_{ij} x_j + F_i)\,\Delta t + r_{0,i}\,\Delta t. \tag{1}$$

Multiple linear regression is applied to find $N_{ijk}, L^{(0)}_{ij}$, and F_i that fit the predictand variables Δx_i. The regression residuals $r_{0,i}$ define the time-dependent stochastic forcing; these residuals typically have long-tailed autocorrelations. Additional model levels are thus included to simulate correlated noise

$$\Delta \mathbf{r}_l = \mathbf{b}_l(\mathbf{x}, \mathbf{r}_0, ..., \mathbf{r}_l)\Delta t + \mathbf{r}_{l+1}\Delta t, \tag{2}$$

for $0 \le l \le L$. The linear maps $\mathbf{b}_l$ are estimated recursively, and the number L of levels is chosen so that the last level $\mathbf{r}_{L+1}$ is well approximated by a spatially correlated white-noise process.

3. Mean phase-space tendencies of the QG3 model

a. The quasi-geostrophic, three-level (QG3) model

Marshall and Molteni's (1993) QG3 model describes the evolution of winds at each of its three pressure-coordinate levels, which represent the lower, middle and upper troposphere. The model is formulated in spherical harmonics and, at a T21 truncation, it has more than a thousand degrees of freedom. Despite its simple form, the QG3 model has a fairly realistic climatology and complex variability; the latter compare favorably with observed atmospheric

behavior (D'Andrea and Vautard 2001; Kondrashov et al. 2004). Franzke et al. (2007) refer to it as a "prototypical GCM," although it is more commonly referred to as an intermediate model, between highly idealized, "toy" models and full GCMs (Ghil and Robertson 2000).

The EMR methodology has been quite successful in reducing this QG3 model to a nonlinear stochastic model with quadratic nonlinearity and a much smaller number of variables on its main level; see Eq. (1). This EMR model accurately reproduces non-Gaussian features of the full QG3 model's probability density function (PDF), as well as the intraseasonal oscillations that characterize the full model's low-frequency variability (Kondrashov et al. 2006; Kravtsov et al. 2009).

b. Mean phase-space tendencies

We combine here several elements from the previous studies of Branstator and Berner (2005) and Franzke et al. (2007) with our EMR methodology, and arrive therewith at a distinctly different approach for the detailed budget analysis of mean phase-space tendencies. First, we define our resolved modes as the leading four EOFs of the daily 500-hPa QG3 field, $\{x_i(t) : 1 \leq i \leq 4\}$, using the streamfunction norm. These EOFs account for more than 30% of variance in the unfiltered daily data (Fig. 1), have the most pronounced deviations from Gaussianity in terms of skewness and kurtosis, and have longer tails in their autocorrelation function (Strounine et al. 2010). Moreover, Kondrashov et al. (2006) established that these EOFs describe the most interesting aspects of the QG3 model's dynamical behavior, oscillatory as well as episodic (cf. Ghil and Robertson 2002), i.e., both its intraseasonal oscillations and multiple regimes.

Second, we derive a nonlinear EMR model based on Eqs. (1) and (2), using the 15 leading streamfunction-norm EOFs, computed from daily 500-hPa streamfunction fields of a 30 0000-day long integration of the QG3 model. This EMR model is essentially the same as that of Kondrashov et al. (2006) and it has $L = 2$ levels. We study 2-component vectors of the mean (daily) tendencies $(< \Delta x_j >, < \Delta x_k >)$, for the six pairs $\{j, k : 1 \leq j, k \leq 4\}$; the averaging operator $< \cdot >$ was applied to all the states that reside in a particular cell of our rectangular partition of each 2-D (x_j, x_k) plane. These 2-vectors of tendencies were estimated from the simulations of the full QG3 model, as well as the reduced EMR. To ensure robust results, we estimated tendencies on a 20 x 20 grid, and only if there were more then 100 states in the particular cell.

Figures 2 and 3 show the mean tendencies of the full QG3 and the EMR model, respectively, in all six planes spanned by the possible pairs of our resolved EOFs. The strikingly good agreement between each pair of corresponding panels in the two figures confirms the EMR model's success in capturing the full QG3 model's mean temporal behavior in phase space. Therefore, to understand the linear and nonlinear contributions to the mean tendencies in the full QG3 model, we can safely use the EMR simulation and the EMR model's empirical dynamics.

The mean flow patterns in the planes spanned by the EOF pairs 1-3 and 2-3 are characterized by the tendencies being antisymmetric for reflections through the origin and having approximately constant speed along ellipsoids. As noted by Branstator and Berner (2005), these features correspond to linear behavior. On the other hand, strongly nonlinear behavior is observed in the four other planes considered, and especially in the EOF 1-4 plane (top-right panel of Figs. 2 and 3), which we will study below in detail. Branstator and Berner

(2005) also noted that the mean tendencies $< \mathbf{x}(t+\tau) > - < \mathbf{x}(t) >$ depend strongly on the lag time τ used for their computation; in particular, the linear component increases with τ. In the present study, however, we are particularly concerned with EMR-modeled daily tendencies ($\tau = \Delta t = 24$ hr), which match nearly perfectly the daily tendencies of the full QG3 model; see again Figs. 2 and 3. As the EMR dynamical operator is explicitly available, the decomposition of the daily tendencies into their various component is explicit and unambiguous.

c. Decomposition of the EMR tendencies

When projected onto the subspace spanned by the four resolved modes, the mean tendencies in Figs. 2 and 3 contain contributions from both the four resolved and the eleven unresolved modes. Given the explicit form of our EMR model's deterministic dynamics, Eq. (1), it is quite straightforward to estimate the relative contributions of the various dynamic terms, both resolved and unresolved, from the time series of the EMR simulations.

The EMR model integration produces surrogate time series that capture the basic statistics of its state vector's evolution, as derived from the QG3 model's time history; these statistics include the means, variances and skewness of each principal component (PC) associated with a given EOF. We obtain therefore $\overline{x_i} = \overline{\Delta x_i} = 0$, when averaged over all possible states in sufficiently long EMR model integrations. Hence the contribution $\overline{V_{Li}}$ of the linear, deterministic portion $L^{(0)}_{ij} x_j$ of the EMR model to the overall time-mean tendency is automatically zero:

$$\overline{V_{Li}(t)} = \overline{L^{(0)}_{ij} x_j} = 0. \tag{3}$$

The individual tendencies $\Delta r_{0,j}(t)$ of the residual stochastic forcing in Eq. (2) do depend on the state vector $\mathbf{x}$. But the contribution to the mean tendencies from the residual stochastic forcing ($< r_{0,j}(t) >, < r_{0,k}(t) >$) is very small in amplitude and largely random. This is true both cell-wise and when averaged over all states, for all six planes spanned by the possible pairs of our resolved EOFs, as shown in Fig. 4. We can thus neglect these unresolved contributions safely in the following analysis.

By time averaging Eq. (1) over all possible states, one thus obtains that the constant terms F_i necessarily equal the average of the nonlinear dynamical contributions:

$$F_i = -\overline{N_{ijk} x_j x_k}, \tag{4}$$

for all j and k. Note that averaging in Eq. (4) reduces to a single sum over the diagonal elements, since the simulated PCs are close to being orthogonal in time, provided the EMR model integration is sufficiently long.

For a given resolved mode $i \leq 4$, we can identify the contribution $V_{R_i}(t)$ to its tendencies $< \Delta x_i >$ that is due solely to the nonlinear interactions within the resolved-mode set Ω of j and k; here $\Omega = \{1 \leq j, k \leq 4\}$ and we sum over it below:

$$R_i = \overline{N_{ijk} x_j x_k}, \qquad V_{R_i}(t) = N_{ijk} x_j x_k - R_i. \tag{5}$$

The remaining nonlinear terms involve interactions either between a resolved and an unresolved mode or between two unresolved modes, i.e. within the set $\overline{\Omega}$ of j, k such that either j or k or both are not in Ω. The corresponding contribution $V_{U_i}(t)$ can be defined accordingly, in a way that is similar to $V_{R_i}(t)$ in Eq. (5):

$$U_i = \overline{N_{ijk} x_j x_k}, \qquad V_{U_i}(t) = N_{ijk} x_j x_k - U_i, \tag{6}$$

by summing over the j, k in $\overline{\Omega}$. Note also that Eqs. (4), (5) and (6) imply necessarily

$$F_i = -R_i - U_i. \tag{7}$$

This force-balancing procedure does not modify in any way the mean tendencies $< \Delta x_i >$ themselves, but ensures a clean interpretation of the results. In particular — by using Eqs. (5), (6), and (7) — one can obtain that the time mean of the full, as well as of the partitioned nonlinear tendencies is zero, similar to Eq. (3):

$$\overline{V_{U_i}(t)} = \overline{V_{R_i}(t)} = \overline{V_{U_i}(t) + V_{R_i}(t)} = 0. \tag{8}$$

d. Further analysis of the EMR tendencies

Figure 5 shows the 2-vectors of the full nonlinear tendencies, including both resolved and unresolved contributions:

$$(< V_{Uj}(t) + V_{Rj}(t) >, < V_{Uk}(t) + V_{Rk}(t) >)\,;$$

the averaging is carried out for all the states that reside in a particular cell of the 20x20-cell partition of each of the six (x_j, x_k) planes of interest. Four of the six mean flow fields exhibit the characteristic double-swirl pattern indicative of strongly nonlinear behavior; the two planes that do not are those spanned by EOFs 1-3 and 2-3, in agreement with the total tendencies shown in Figs. 2 and 3.

Figure 6 presents the fully resolved nonlinear tendencies $(< V_{Rj}(t) >, < V_{Rk}(t) >)$. The difference between it and Fig. 5 is very small for all planes where nonlinear swirls are strong, namely the planes spanned by EOFs 1-2, 1-4, 2-4 and 3-4. Clearly, the effect of the nonlinear tendencies V_{U_i} that involve unresolved modes is also very small for these pairs.

In order to refine further our interpretation of nonlinear signatures, we have repeated the analysis of Figs. 5 and 6 by defining as resolved only the pair of EOFs that span a particular 2-D plane, and the other 13 modes as unresolved. For example, in the case of the EOF 1-3 plane, the nonlinear resolved tendencies would be only those that involve the x_1^2, x_1x_3, and x_3^2 interactions; see again Eq. (5). Even though such a definition of the resolved modes is quite similar to that of Franzke et al. (2007), the results are entirely different: The nonlinear tendencies due to interaction between the resolved modes alone, as shown in Fig. 7, are very similar to the full nonlinear tendencies in Fig. 5, as well as to the tendencies due to the interactions between all four leading EOFs in Fig. 6. Thus the interaction with the unresolved modes is quantitatively quite minor, even when choosing only two modes as resolved, but according to the EMR methodology.

Figure 8 presents a detailed analysis of linear and nonlinear contributions to the mean phase-space tendencies in the plane spanned by EOFs 1-4, in which the nonlinear double-swirl pattern — as seen in Figs. 8a and 8b — is especially strong. This pattern is strikingly absent, however, in Figs. 8c and 8d. The results in Fig. 8c correspond to a linear EMR model, with $N_{ijk} \equiv 0$ in Eq. (1), and are fairly close to being perfectly antisymmetric about the origin, in agreement with Branstator and Berner's (2005) results. This antisymmetry can be explained by the following two LIM properties: (i) simulated tendencies are invariant under the mirror transformation $x_i \rightarrow -x_i$, when $F_i \approx 0$, cf. Eq. (1); and (ii) x_i is normally distributed for $L = 1$.

On the other hand, the linear contribution in our quadratic EMR model, shown in Fig. 8d, is not perfectly antisymmetric. This can be explained by the non-gaussianity of the PC-1 time series that is simulated by a nonlinear EMR model; the latter, in turn, is consistent

with non-gaussianity of the full QG3 model's time series. The positive skewness of the PC-1 time series in Fig. 1b leads to violation of the mirror invariance under $x_i \to -x_i$ in the estimated linear tendencies. Figure 8 thus further confirms the dominant contribution of the resolved nonlinear interactions to the QG3 model's tendencies.

4. Concluding remarks

We used nonlinear stochastic models obtained by empirical model reduction (EMR) as a diagnostic tool for studying effects of linear and nonlinear dynamics in a fairly realistic intermediate climate model, the quasi-geostrophic, three-level (QG3) model of Marshall and Molteni (1993). An EMR model with quadratic nonlinearity, driven by data-derived colored noise, was constructed in the phase subspace spanned by the 15 leading EOFs of the QG3 model at T21; see Eq. (1). This model, with the colored noise represented by a two-level parametrization, cf. Eq. (2), reproduces nearly perfectly the daily-mean tendencies of the full, high-dimensional QG3 model.

The nonlinear features of these tendencies are dominated by the EMR-parameterized, deterministic interactions between the four leading EOF modes. The interactions with trailing EOFs are therefore linearly parameterizable as the multi-level noise, and do not significantly contribute to the model's nonlinear characteristics. This result is further buttressed by showing that for a particular 2-D plane — in which the double-swirl patterns in the mean tendencies of the full QG3 model are strong — these signature patterns do occur mostly due to the nonlinear interactions between the pair of EOFs that span such a plane. The same holds for other planes of this type (not shown).

These findings should be contrasted with the results of Franzke et al. (2007), who used a different norm to define the EOFs and an entirely different strategy to compute the state-averaged mean tendencies. The EMR results are not qualitatively sensitive to the norm used for data compression; see Strounine (2007) and Strounine et al. (2010).

On the other hand, using an EMR model to define those interactions that are linearly parameterizable vs. those that are not — in terms of their contribution to the daily-mean state-averaged tendencies, cf. Kravtsov et al. (2009) — is likely to be the primary reason for differences in interpretation between our study and that of Franzke et al. (2007). The latter defined the tendencies based on state-averaged instantaneous contributions from various linear and nonlinear terms of the full QG3 model's operator. We conclude therefore that the way of defining interactions between the resolved and unresolved modes plays a crucial role in the dynamical interpretation of the tendency-based statistical diagnostics. An additional ingredient in this distinction is the number of resolved modes, which equals four in the present study vs. two in Franzke et al.'s (2007) study.

Acknowledgments.

It is a pleasure to acknowledge exchanges with M. D. Chekroun, G. Branstator, C. Franzke and A. J. Majda on topics related to this study. We also thank two anonymous reviewers for their constructive comments. This work was supported by the Office of Science (BER), U. S. Department of Energy (DOE), under grants DE-FG02-07ER64439 and DE-FG02-07ER64429 at UCLA, and by DOE grant DE-FG02-07ER64428 and NSF grant ATM-0852459 at UWM.

REFERENCES

Branstator, G. and Berner, J., 2005: Linear and nonlinear signatures in the planetary wave dynamics of an AGCM: Phase space tendencies. *J. Atmos. Sci.*, **62**, 1792–1811.

D'Andrea, F. and R. Vautard, 2001: Extratropical low-frequency variability as a low-dimensional problem. Part I: A simplified model. *Quart. J. Roy. Meteor. Soc.*, 127, 1357–1374.

Franzke, C. and A. J. Majda, 2006: Low-order stochastic mode reduction for a prototype atmospheric GCM. *J. Atmos. Sci.*, **63**, 457–479.

Franzke, C., Majda, A. J. and Branstator, G., 2007: The origin of nonlinear signatures of planetary wave dynamics: Mean phase space tendencies and contributions from non-Gaussianity. *J. Atmos. Sci.*, **64**, 3987–4003.

Ghil, M., and A. W. Robertson, 2000: Solving problems with GCMs: General circulation models and their role in the climate modeling hierarchy, in *General Circulation Model Development: Past, Present and Future*, D. Randall (Ed.), Academic Press, San Diego, pp. 285–325.

Ghil, M., and A. W. Robertson, 2002: "Waves" vs. "particles" in the atmosphere's phase space: A pathway to long-range forecasting? *Proc. Natl. Acad. Sci. USA*, **99** (Suppl. 1), 2493–2500.

Kondrashov, D., K. Ide, and M. Ghil, 2004: Weather regimes and preferred transition paths in a three-level quasigeostrophic model, *J. Atmos. Sci.* **61**, 568–587.

Kondrashov, D., S. Kravtsov, and M. Ghil, 2006: Empirical mode reduction in a model of extratropical low-frequency variability, *J. Atmos. Sci.*, **63**, 1859-1877.

Kondrashov, D., S. Kravtsov, A. W. Robertson and M. Ghil, 2005: A hierarchy of data-based ENSO models. *J. Climate*, **18**, 4425–4444.

Kravtsov S., D. Kondrashov, and M. Ghil, 2005: Multi-level regression modeling of nonlinear processes: Derivation and applications to climatic variability. *J. Climate*, **18**, 4404–4424.

Kravtsov S., D. Kondrashov and M. Ghil, 2009: Empirical model reduction and the modeling hierarchy in climate dynamics, in *Stochastic Physics and Climate Modelling*, T. N. Palmer and P. Williams (Eds.), Cambridge Univ. Press, pp. 35–72.

Majda, A. J., I. Timofeyev, and E. Vanden-Eijnden, 2003: Systematic strategies for stochastic mode reduction in climate. *J. Atmos. Sci.*, **60**, 1705–1722.

Majda A. J., C. Franzke and B. Khouider, 2008: An applied mathematics perspective on stochastic modelling for climate, *Phil. Trans. R. Soc.*, **366**, 2427–2453.

Marshall, J. and Molteni, F., 1993: Toward a dynamical understanding of atmospheric weather regimes. *J. Atmos. Sci.*, 50, 1792–1818.

Penland, C., 1996: A stochastic model of Indo-Pacific sea-surface temperature anomalies. *Physica D*, **98**, 534–558.

Selten, F.M. and G. Branstator, 2004: Preferred regime transition routes and evidence for an unstable periodic orbit in a baroclinic model *J. Atmos. Sci.*, **61**, 2267–2282.

Strounine, K., 2007: Reduced Models of Extratropical Low-Frequency Variability. Ph.D. Thesis, Department of Atmospheric and Oceanic Sciences, University of California, Los Angeles.

Strounine, K., S. Kravtsov, D. Kondrashov and M. Ghil, 2010: Reduced models of atmospheric low-frequency variability: parameter estimation and comparative performance, *Physica D*, **239**, pp 145–166.

List of Figures

7 Same as in Fig. 6, but when resolved nonlinear interactions include *only those* two EOFs that span a particular EOF plane. 25

8 Detailed budget of mean phase-space tendencies for the plane spanned by EOFs 1 and 4: (a) tendencies due to the EMR model's full nonlinear operator; (b) nonlinear resolved contribution of the EMR model; c) LIM fit; and (d) linear tendencies of the nonlinear EMR. 26

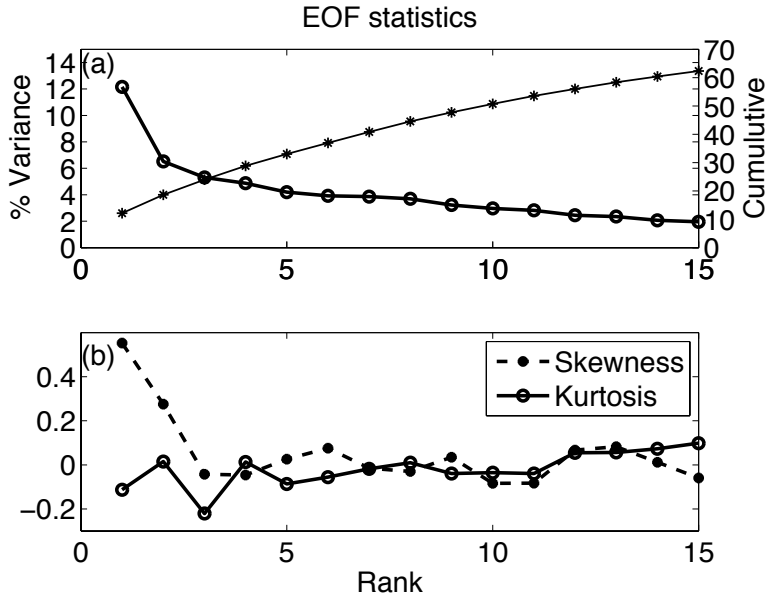

FIG. 1. Basic statistics of the empirical orthogonal functions (EOFs) of the daily data from the QG3 model's 30 000-day long integration; shown are results for the 500-hpa EOFs in the streamfunction norm. (a) Individual variance (heavy solid) and cummulative variance (light gray); (b) skewness and kurtosis of the corresponding principal components (PCs), as indicated in the panel legend. While there is no clear break in the variance, the two indicators of non-Gaussianity in the lower panel indicate that the four leading PCs are substantially non-Gaussian, while the other PCs are essentially Gaussian, within sampling error.

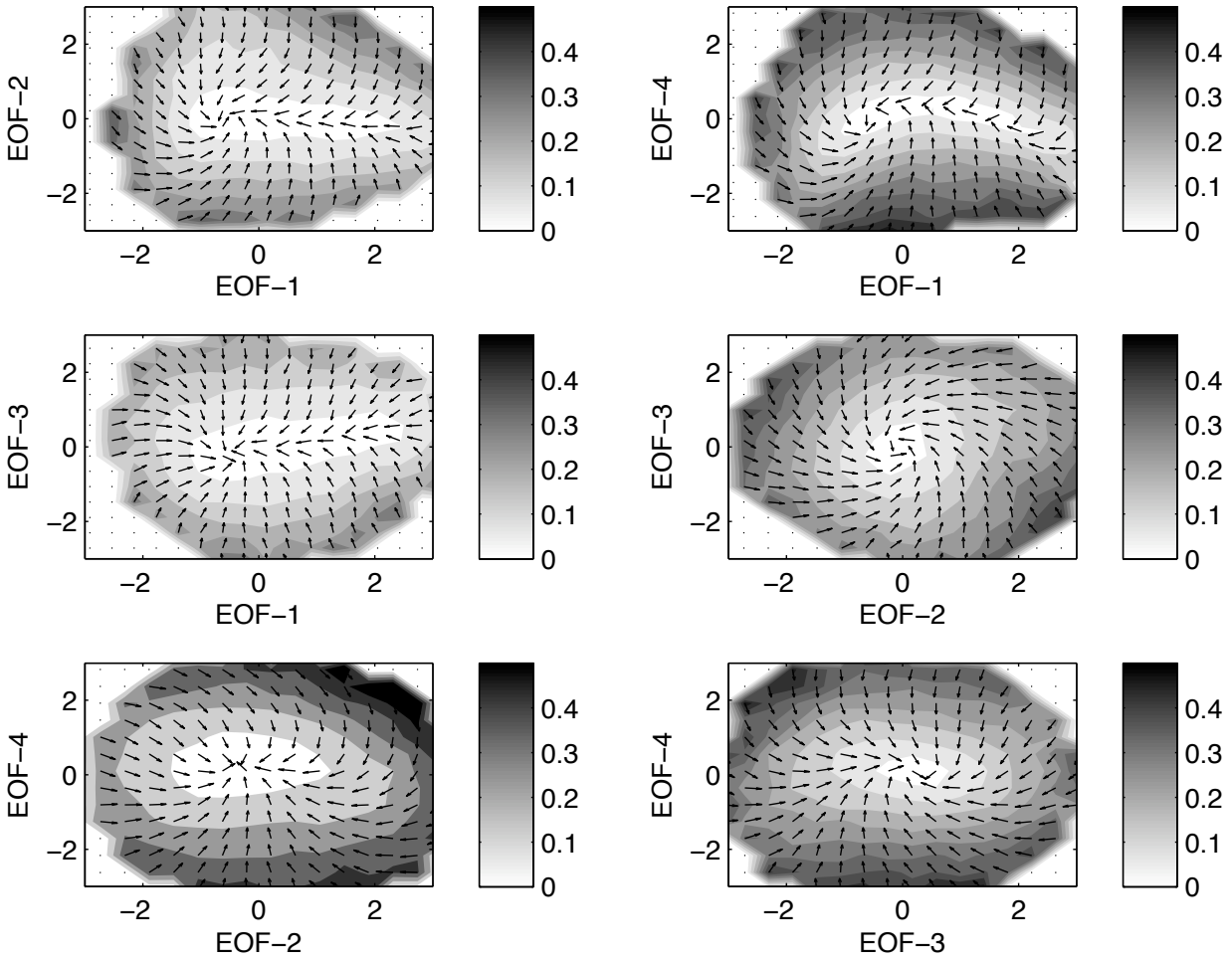

FIG. 2. Mean phase-space tendencies for the 500-hpa streamfunction-norm EOFs of the QG3 model's daily data. Here and in all subsequent figures, shading indicates the magnitude of the tendencies in unit standard deviation per day (1 std dev day^{-1}), and arrows are normalized to have the same length.

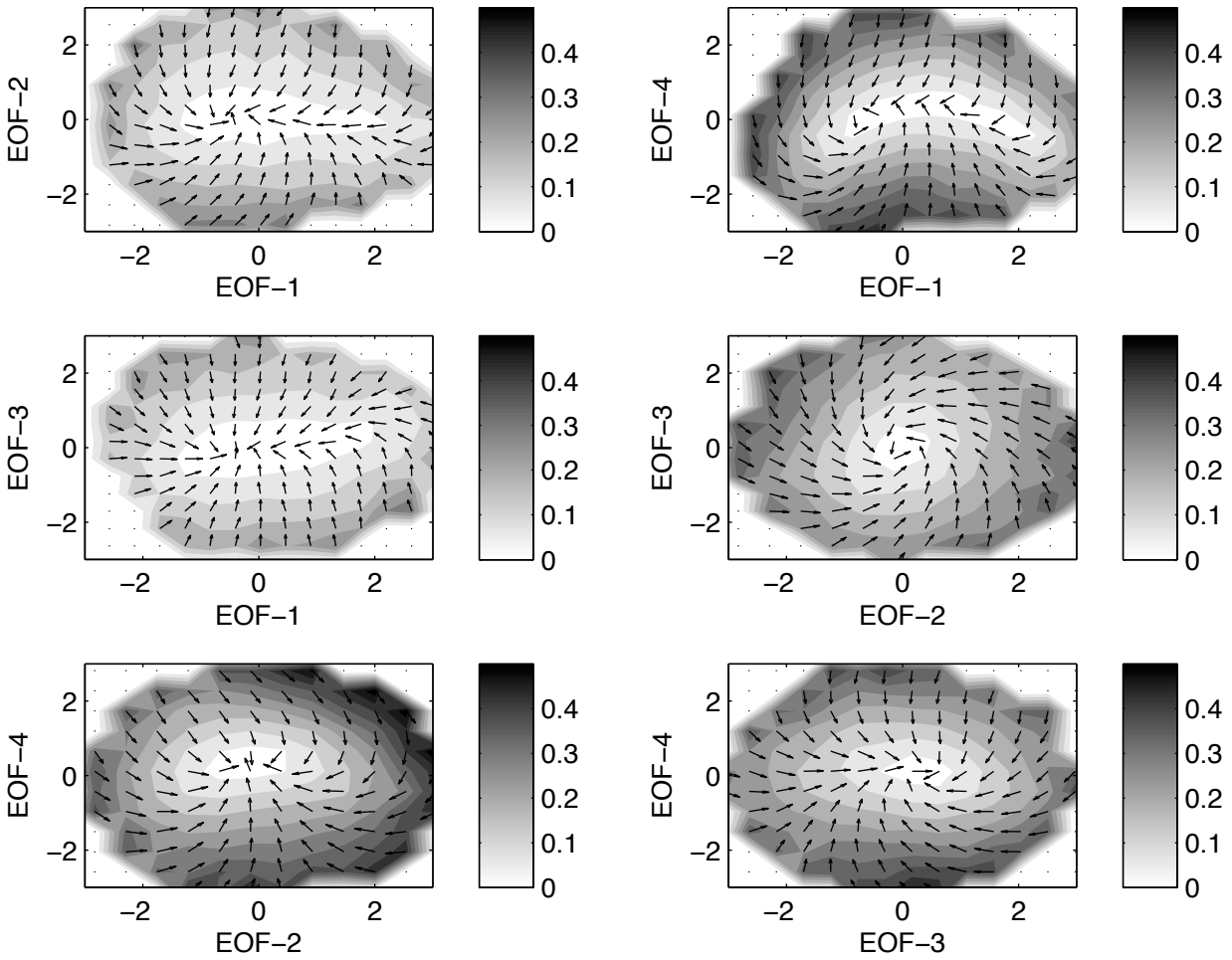

FIG. 3. Same as Fig. 2, but for the for the nonlinear EMR model.

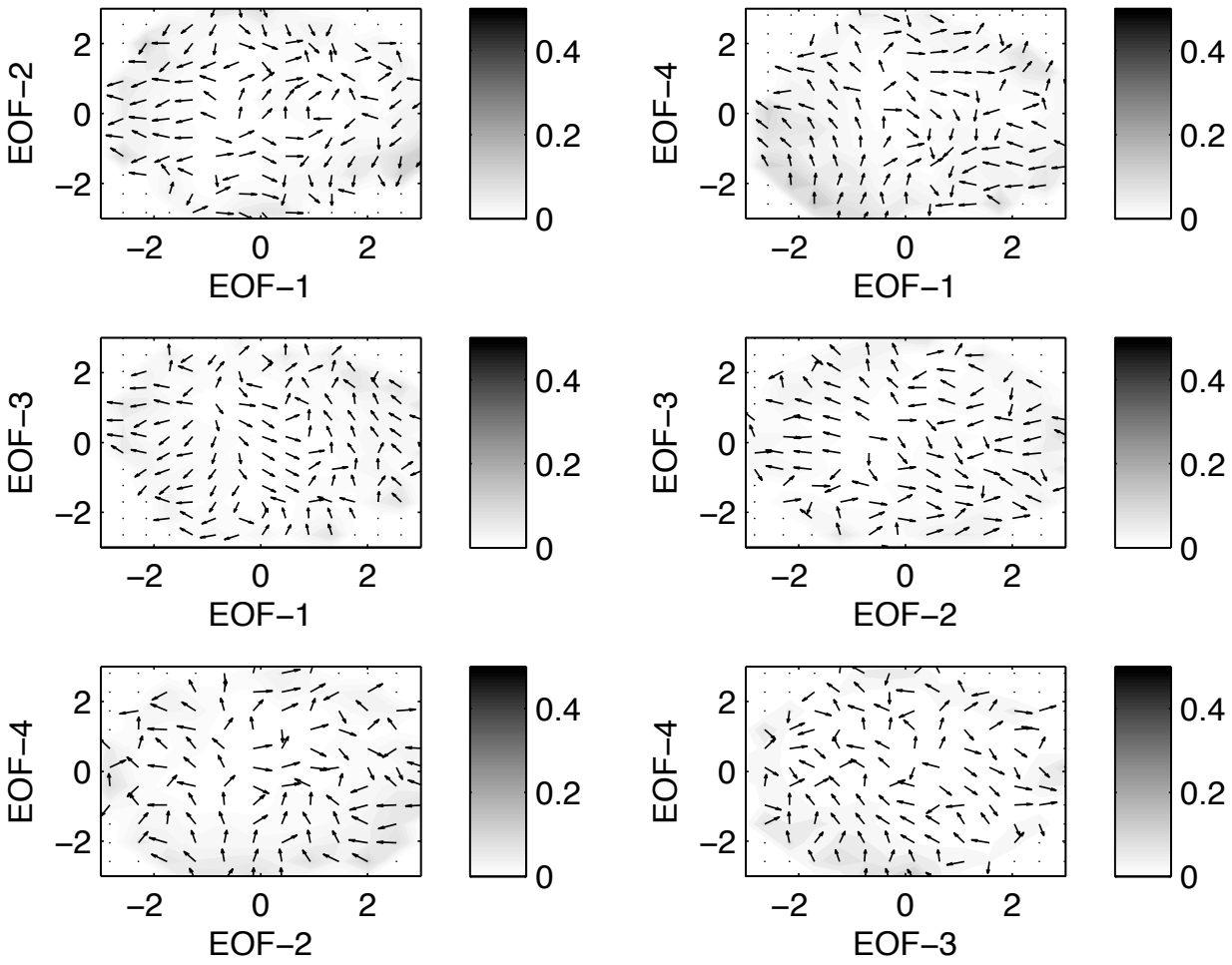

FIG. 4. The contribution to the mean tendencies from the stochastic forcing $(< r_{0,j}(t) >, < r_{0,k}(t) >)$; see Eq. (1).

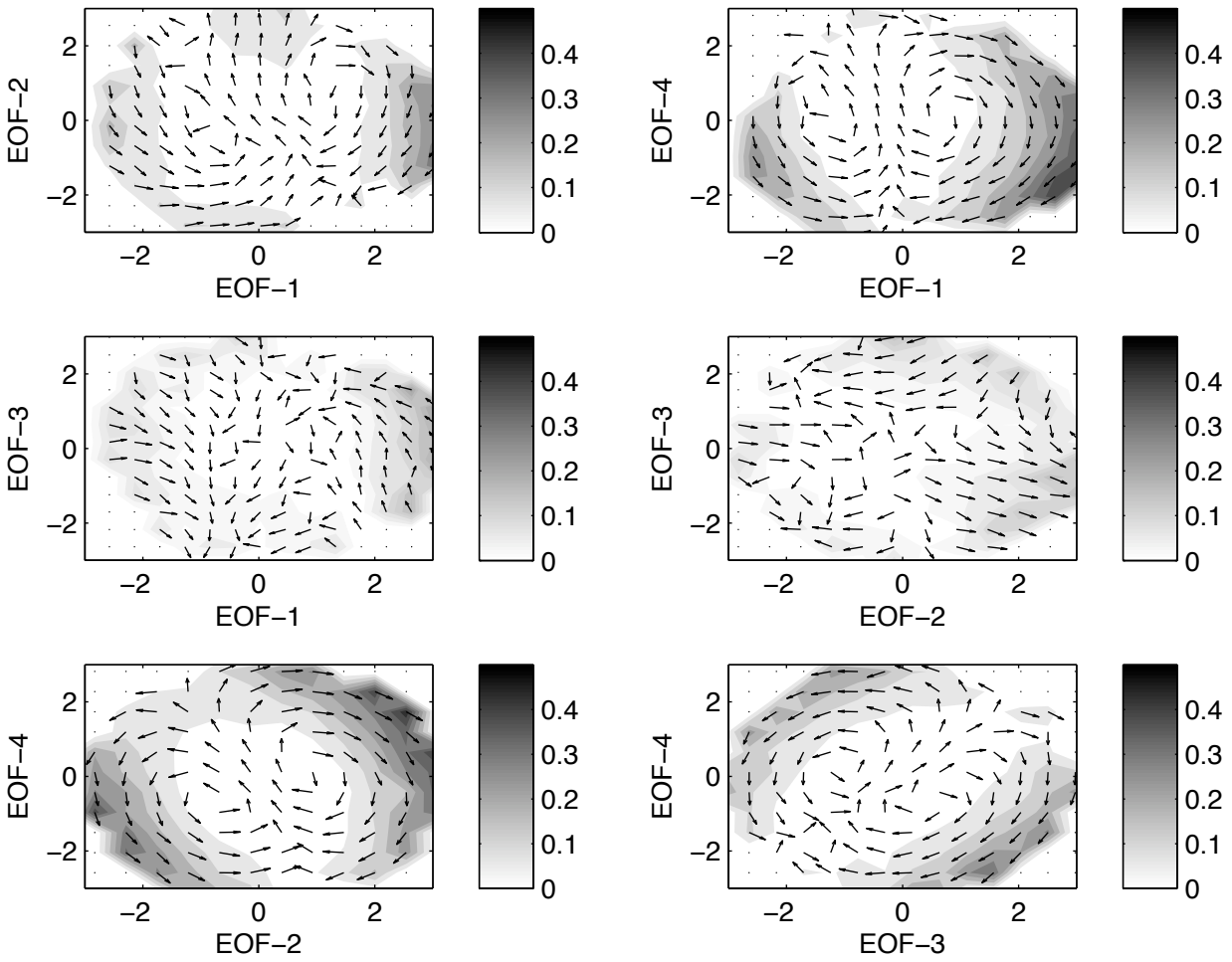

FIG. 5. Mean phase-space tendencies $\left(< V_{R_j}(t) + V_{U_j}(t) >, < V_{R_k}(t) + V_{U_k}(t) >\right)$; see Eqs. (5) and (6), due to the EMR model's full nonlinear operator.

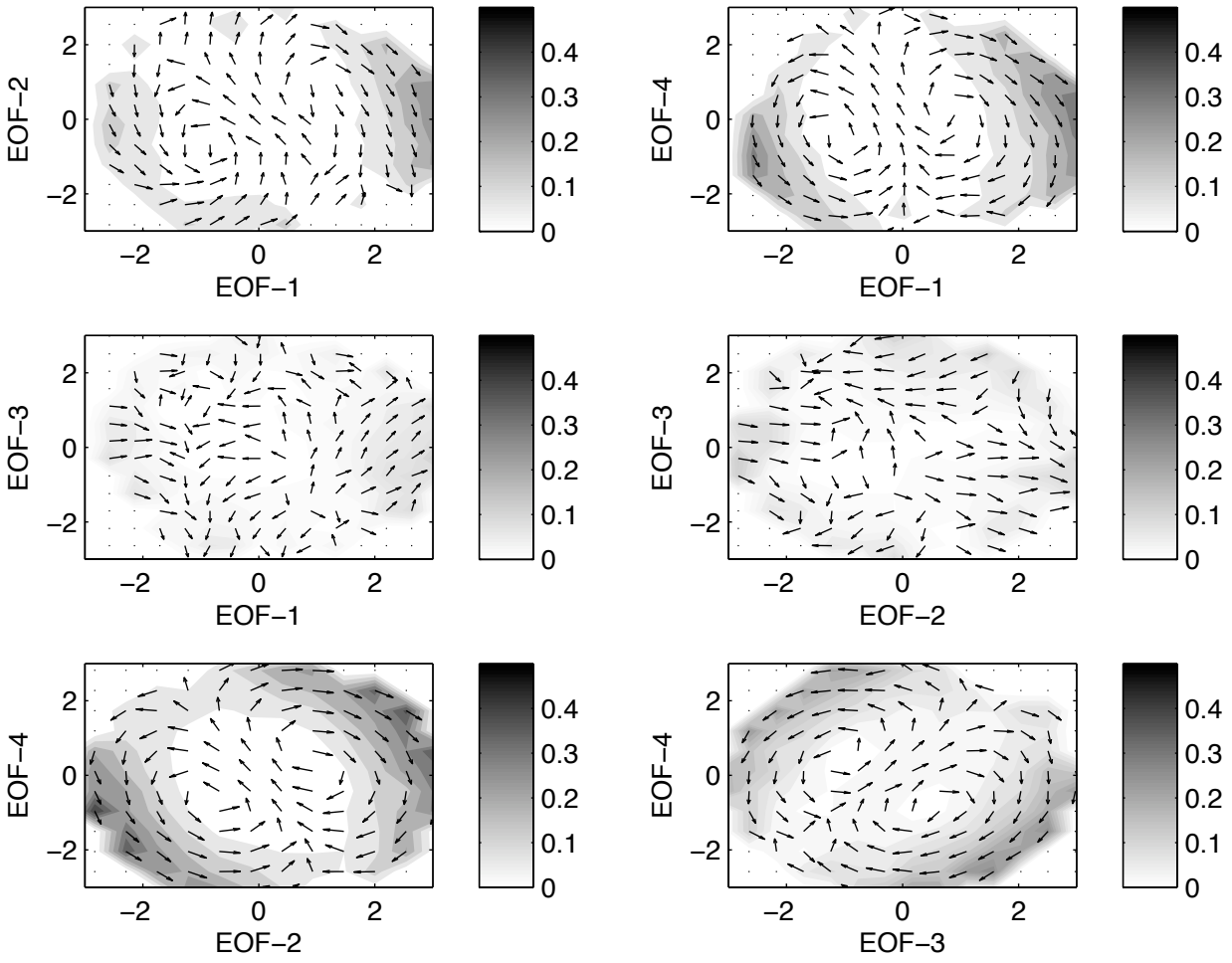

FIG. 6. Mean phase-space tendencies $\left(< V_{R_j}(t) >, < V_{R_k}(t) >\right)$; see Eq. (5), due only to the resolved interactions between the four leading EOFs in the EMR model's nonlinear operator.

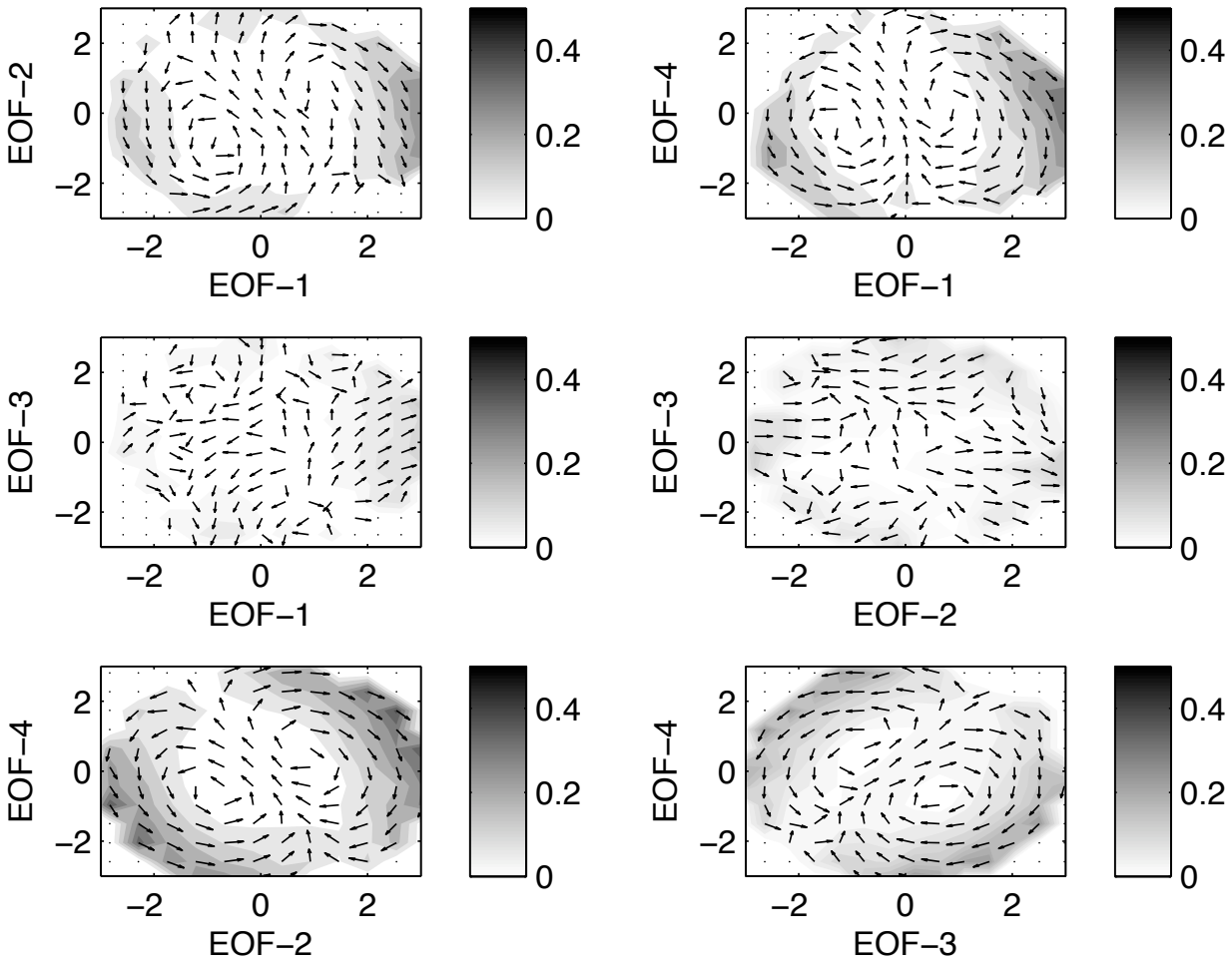

FIG. 7. Same as in Fig. 6, but when resolved nonlinear interactions include *only those* two EOFs that span a particular EOF plane.

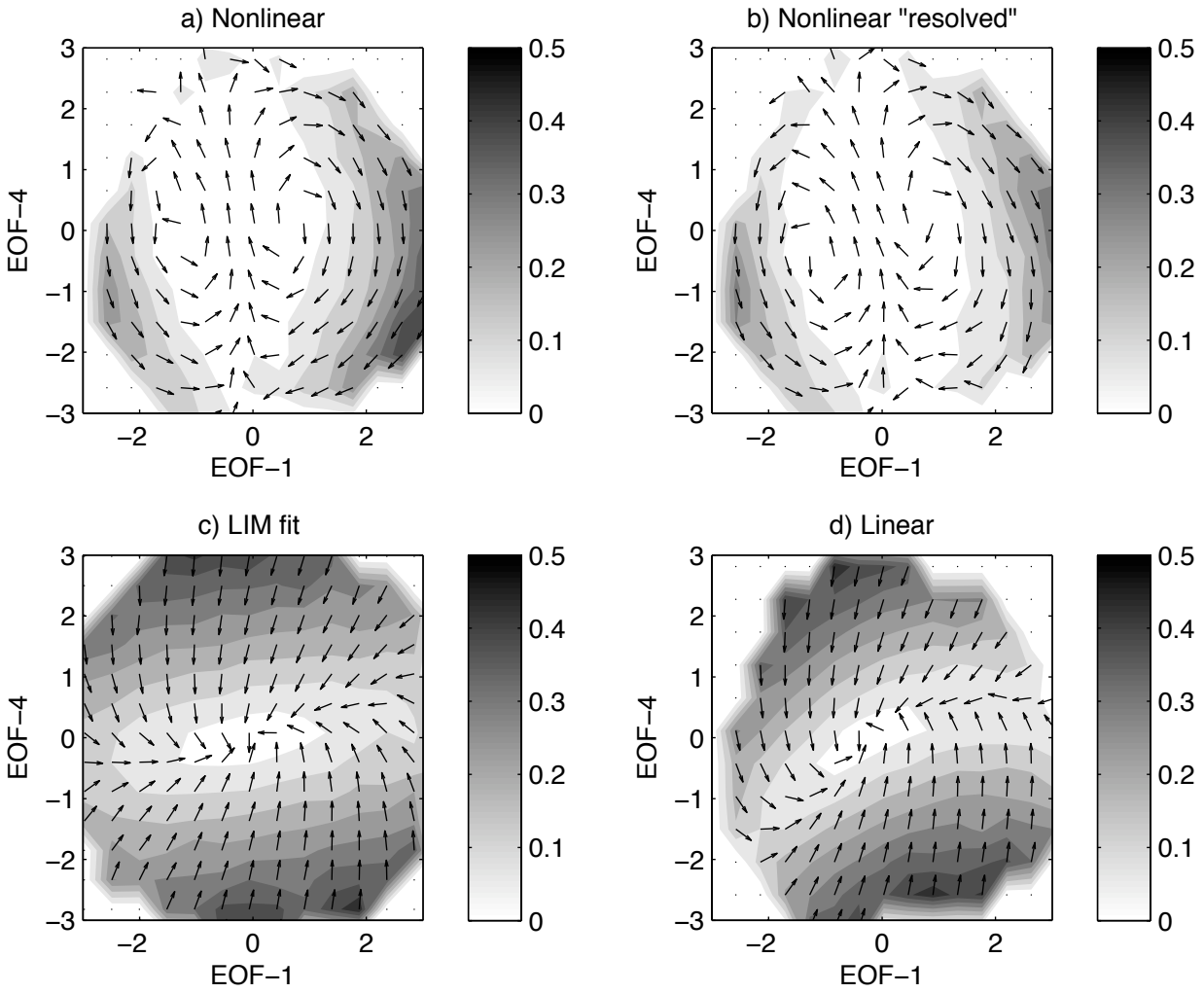

FIG. 8. Detailed budget of mean phase-space tendencies for the plane spanned by EOFs 1 and 4: (a) tendencies due to the EMR model's full nonlinear operator; (b) nonlinear resolved contribution of the EMR model; c) LIM fit; and (d) linear tendencies of the nonlinear EMR.